Available online at www.sciencedirect.com
SCIENCE DIRECT®
Pergamon
International Journal of Machine Tools & Manufacture 43 (2003) 1383–1390
INTERNATIONAL JOURNAL OF MACHINE TOOLS & MANUFACTURE
DESIGN, RESEARCH AND APPLICATION

Wavelet transform analysis of acoustic emission in monitoring friction stir welding of 6061 aluminum

Changming Chen, Radovan Kovacevic *, Dragana Jandgric

Research Center for Advanced Manufacturing, Department of Mechanical Engineering, Southern Methodist University, 1500 International Parkway, Suite 100, Richardson, TX 75081, USA

Received 4 February 2003; received in revised form 28 April 2003; accepted 7 May 2003

Abstract

In this paper, acoustic emission (AE) signals are detected and preliminarily analyzed in order to investigate the possibility of applying the AE technique for the in-process monitoring of an entire friction-stir-welding (FSW) process. Experimental tests are carried out using a high-speed rotating tool traversing on two, butted 6061 aluminum alloy plates with three equally spaced gaps made of two notches aligned along the butting joint of the parts. The wavelet transform (WT) is used to decompose the AE signal into various discrete series of sequences over different frequency bands. There are significant sudden changes in the band energy at the moment when the probe penetrates into and pulls out of the weld joint, as well as when the shoulder makes contact with or detaches from the plates. The band energy variation during the traversing of the tool over the defected region reflects the existence, location, and size of the weld defects. A three-dimensional representation of band energy vs time and scale gives valuable information on the potential weld defects during friction stir welding. Coupled with a contour mapping, the representation can be effectively utilized for monitoring the transient welding state and quickly identifying gap defects.

Keywords: Acoustic emission; Wavelet analysis; Friction stir welding; Process monitoring; Weld defects

1. Introduction

Friction-stir-welding (FSW) is a solid-state material joining method resulting in a low-level of deformation in the workpieces. As this novel jointing method rapidly expands its application in joining aluminum alloys, steel, and titanium [1,2], the monitoring of joining the weld quality and welding process has become more important. In unattended manufacturing processes, the tool condition and material quality are evaluated based on statistical data. Such a procedure sometimes may not be efficient since an accidental tool breakage and/or sudden change of processing parameters can decrease the system productivity and deteriorate the material performance. An in-process sensing technique allows for real-time monitoring of the tool condition and product quality, which provides for a more flexible automation in manufacturing [3].

AE monitoring is one of the most sensitive techniques that is useful for real-time detection of crack mode and kinetics in various materials [4]. The AE technique has been used for monitoring the cutting tool wear [5], the wear rate of materials [6], and for an estimation of the workpiece quality [7]. There is no available published data on using the AE technique to monitor the FSW process. The big problem in using AE to monitor FSW is that a large amount of components involved in the acquired AE signals are generated from the friction between the shoulder and the workpiece, which makes for a very difficult extraction of valuable features from AE signals.

The signals acquired during FSW are found to be time-variant, and a time-frequency analysis with fast Fourier transform (FFT) is not appropriate for this case. In theory, the time-variant AE signals generated in the FSW should contain many of the informative features related to the material quality and welding state;

* Corresponding author. Tel.: +1-214-768-4873; fax: +1-214-768-0812.
E-mail address: kovacevi@seas.smu.edu (R. Kovacevic).

0890-6955/$ - see front matter © 2003 Elsevier Ltd. All rights reserved.
doi:10.1016/S0890-6955(03)00130-5

Nomenclature

t	time (s)
$x(t)$	AE signal function of time
$W^x_{a,b}$	wavelet transform of signal $x(t)$
α	normalization factor
a	translation parameter in scale (each scale represents a frequency band)
b	translation parameter in time
$\psi(t)$	basis function
BE^a_x	band energy corresponding to scale a
A1–A6	approximation levels (low-pass filters)
D1–D6	detail levels (high-pass filters)

although, there is no straightforward method to correlate the frequency of the signal to specific defects of materials. This research will focus on the investigation of the time-frequency properties of AE signals using a wavelet transform and the recognition of features related to the tool movement states and weld quality.

2. Introduction of wavelet transform

WT utilizes its basis, known as wavelets, and performs a decomposition of the signal $x(t)$ into a weighted set of scaled wavelet functions $\psi(t)$. In general, for a function of $x(t)$ in L(IR), the wavelet transform energy can be defined by [8]:

$$W^x_{a,b} = |\alpha|^{-1/2} \int_{-\infty}^{+\infty} x(t)\psi\left(\frac{t-b}{a}\right)\mathrm{d}t \tag{1}$$

in which, α is a normalization factor, $\psi(t)$ is the mother wavelet with the scale parameter a (a, corresponds to a frequency band, Δ_a), and the shift parameter b that provides a set of localized functions both in frequency and time.

Unlike the Fourier transform that gives the precise frequency information, the wavelet transform provides band frequency information in the time domain. The band energy at the scale a can be computed by:

$$BE^a_x = \int_{-\infty}^{+\infty} |w^x_{a,b}|^2 \mathrm{d}t. \tag{2}$$

Unlike bandpass filtering where the bandwidth is constant, in WT, the band energy at each scale represents a different bandwidth. Wavelets at a high frequency are of short duration, and wavelets at low frequency are of relatively good frequency resolution. The varying 'window' structure of the WT is related to the resolution presented by rectangles on the time-frequency plane, as shown in Fig. 1. The characteristics of WT makes this method more appropriate for the analysis of complex signals such as transient and abrupt changes that are generally the symptoms of defects or sudden changes of the processing state.

3. Experimental procedure

The FSW system with a high-speed rotating tool was used to weld butted plates as shown in Fig. 2. The tool consisted of a shoulder with a diameter of 24 mm, and a threaded probe with a diameter of 6 mm and a height of 5.5 mm. An on-line emission monitoring system was used to detect the welding state and evaluate the weld quality during the probe penetration, welding, and probe pullout. The two AE sensors were arranged symmetrically on both sides of the butting joint of the parts with a distance of 70 mm to the butting line, and moved along

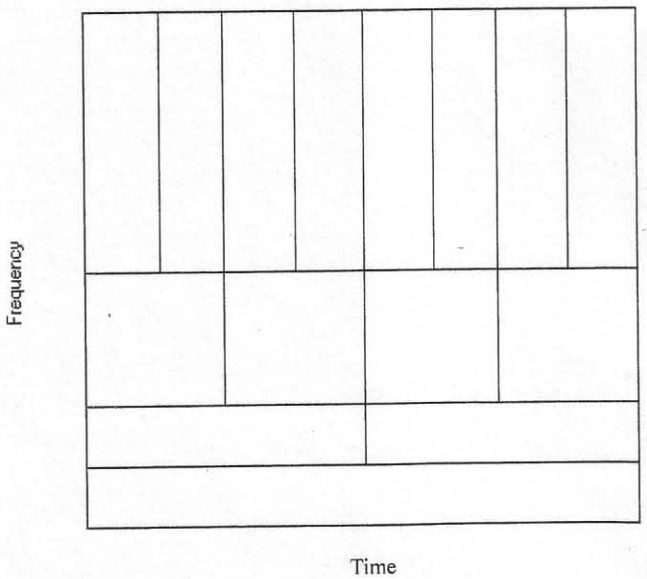

Fig. 1. Wavelet transform—time and frequency resolution.

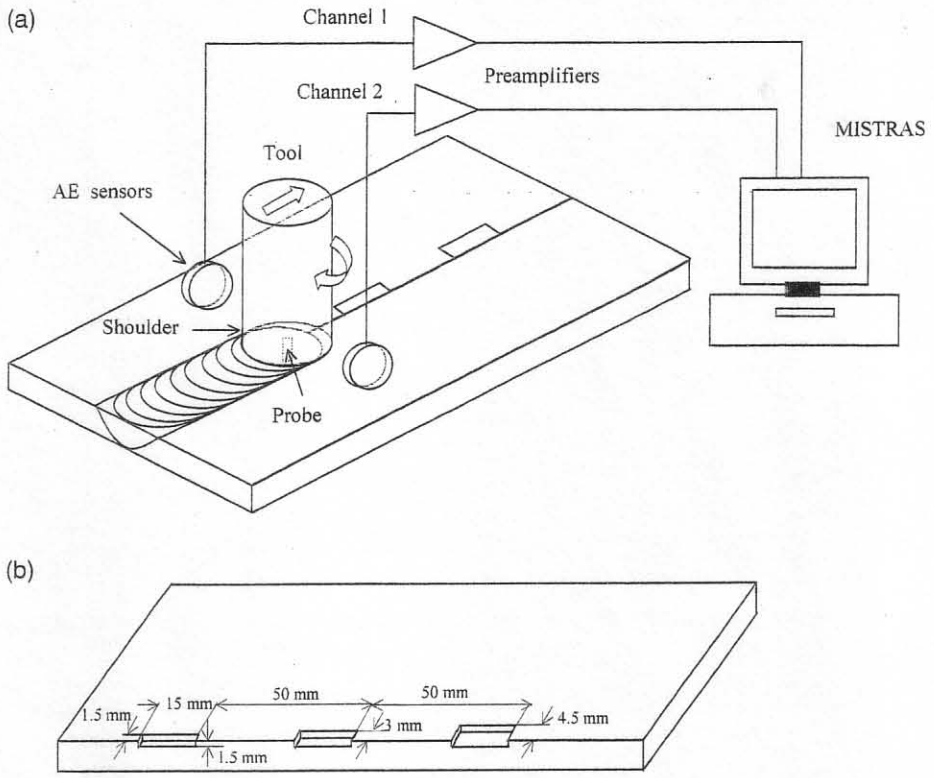

Fig. 2. Diagram of the (a) experimental setup and (b) test plate with three notches made along the edge.

the welding direction with the tool. The AE couplants between the top surface of the welded plate and the sensors were silicone rubber. The sampling rate was 1 MHz. Preliminary AE test results recorded on the butted plates while the plates were not being welded but the machine was in the running mode were found to contain noises at frequencies below 20 kHz, which are attributed to the machine vibration. In order to filter out this mechanical noise from the AE signal, a 20-kHz high-pass filter was applied. The AE signals data from the two sensors (channel 1 and channel 2) were found to have the same frequency and amplitude response by calibration. The generated acoustic emission data during welding was collected for the entire welding process, progressively amplified through the preamplifier with a 40-dB gain and 20-kHz high-pass filter, and transmitted to the signal processor.

Two, 6061-T6 aluminum alloy plates with a thickness of 6.5 mm and a width of 100 mm were friction stir welded along the butting joint. Each of the two butted plates was preliminarily machined to have three notches spaced equally along the joint edge with sizes of 15 $\times$1.5 $\times$ 1.5, 15 $\times$ 3.0 $\times$ 1.5 and 15 $\times$ 4.5 $\times$ 1.5 mm, respectively. Each of the three notches was arranged symmetrically on both sides of the joint line. The tool traversing speed and rotating speed were selected as 200 mm/min and 344 rpm, respectively. These selected parameters have provided good microstructure and mechanical properties in our preliminary experiments.

4. Results and discussion

In this paper, Daubechies wavelets with an order of six are used to decompose the signals, and the band energies at different scales are computed by Eq. (1).

4.1. Analysis of signals acquired during static FSW process

In this experiment, the signals were collected by two channels during the static FSW process that consists of: the probe penetrates; the shoulder makes contact with the top surface of the plate; the tool dwells for 15 s under a down force; the shoulder detaches from the plate; and the probe detaches from the plate.

Fig. 3 shows the band energy of the AE signal vs time at different scales for signals collected through channels 1 and 2 during the entire static FSW process. Distinct peak features are spotted at the beginning of the probe penetration, at the contact of the shoulder with the workpieace, and at the detachment of the shoulder and probe from the workpiece. The distinctive features in the plots are thought to be caused mainly by the friction between the parts in contact, and thermomechanical process of the welded material. Song et al. [9] conducted a numerical modeling of the temperature history during probe penetration, and found that the temperature near the tool probe increases rapidly while the probe plunges into the workpiece. An expanding thermoactivated deformation

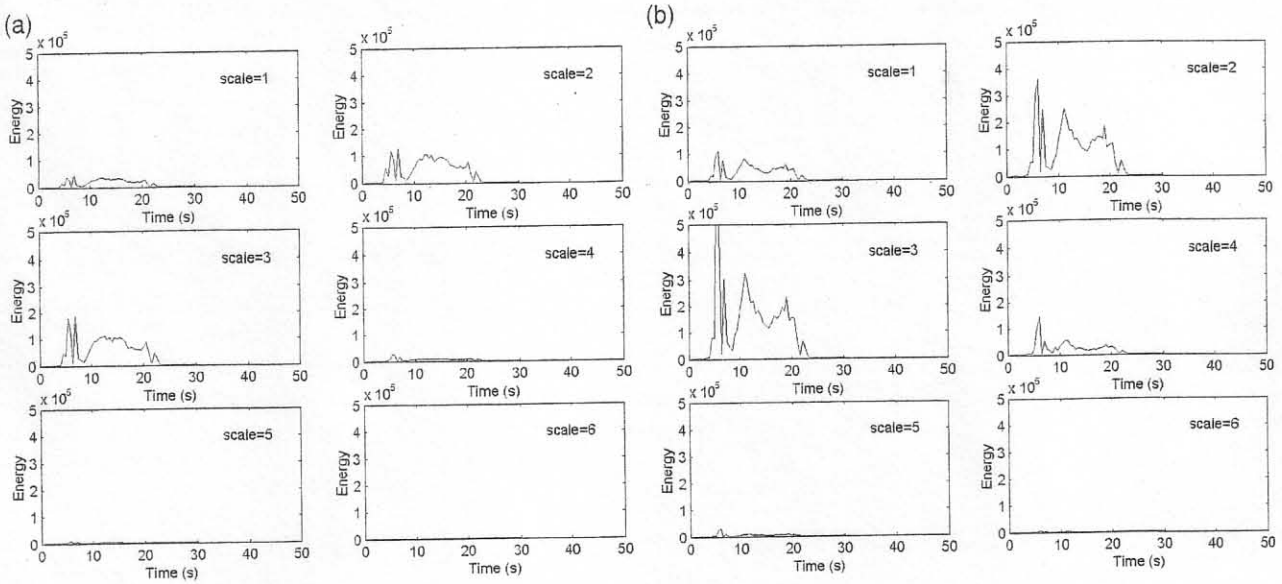

Fig. 3. Band energy vs time at different scales for AE signals collected during entire FSW process through (a) channel 1 and (b) channel 2.

is believed to occur in the proximity of the probe. An investigation of AE during the annealing of the preliminary strained polycrystalline aluminum shows that at the low-temperature range (20–250 °C), the AE intensity increases to a peak value and then decreases monotonically [10]. Further increasing the annealing temperature to 600 °C leads to a gradual increase in the AE intensity then decreases due to the decreasing rate of migration of the grain boundaries [10]. The AE features that occur in the low-temperature range are related to the high-energy defects such as stacking faults and dislocations, while those occurring at high-temperatures are related to migration of grain boundaries [10].

The variation in the AE intensity during 10–20 s in Fig. 3 can be explained by the similar evolution of defects and boundary movement in the strained welded parts during the heating that is derived from friction between the tool and workpiece under a down force. Fig. 4 shows typical microstructures of a weld cross section perpendicular to the welding direction. The nugget zone shown in the Fig. 4(b) features large amounts of precipitates mainly dispersed at the boundaries of the grains. The precipitates are thought to be caused by a dynamic recrystallization of the plasticized weld zone (nugget) with a maximum temperature of 425 °C [11]. The grains in the heat-affected zone (HAZ) are seriously coarsened by the heat flux from the tool, which is shown in the Fig. 4(c). Compared with the heat-unaffected zone of 6061-Al alloy shown in the Fig. 4(d), it is obvious that the stir effect and the derived heat produce a recrystallization of precipitates and grain growth in the actual weld zone. Murr et al. [11] did a transmission electron microscopy (TEM) examination of a 6061-Al weld, and found that the dislocations of the precipitates decreased after welding, when compared with the base material led to the softening of the weld. All these effects are expected to account for the changes in AE signals.

The peaks appearing after 20 s in Fig. 3 correspond to the detachment of the shoulder and probe from the workpiece, respectively. Compared with the energy of signals collected at channels 1 and 2, it is evident that the energy in channel 2 (the retreating side) is larger than that in channel 1 (the advancing side). This difference indicates a difference in flow pattern and deformation evolution between the advancing side and the retreating side of the material during welding.

The results of the WT analysis can be represented as three-dimensional profile and contour map of band energy vs time and scale. Fig. 5 shows a wavelet profile and contour map of the AE signals for tool penetration and pullout. The three-dimensional wavelet profile in Fig. 5 is a collection of band energy for a given set of the scale (or frequency) and time, which shows distinct features matching the beginning of penetration and pullout of the tool from this prospective. This type of presentation is helpful in identifying general trends of the time-frequency characteristic.

The contour map in Fig. 5 corresponds to the wavelet intensity of the transform at points in the scale-time plane, displaying how the signal intensity of a different particular band frequency changes simultaneously with time. It is obvious that the probe begins to contact with the samples at 6 s, and the main energy is in the frequency region of scale 1–4 with a peak at scale 3.

4.2. Analysis of AE signals acquired for weld with gap defects

The AE signals were acquired during tool traversing in the welding direction at a speed of 200 mm/min. Fig.

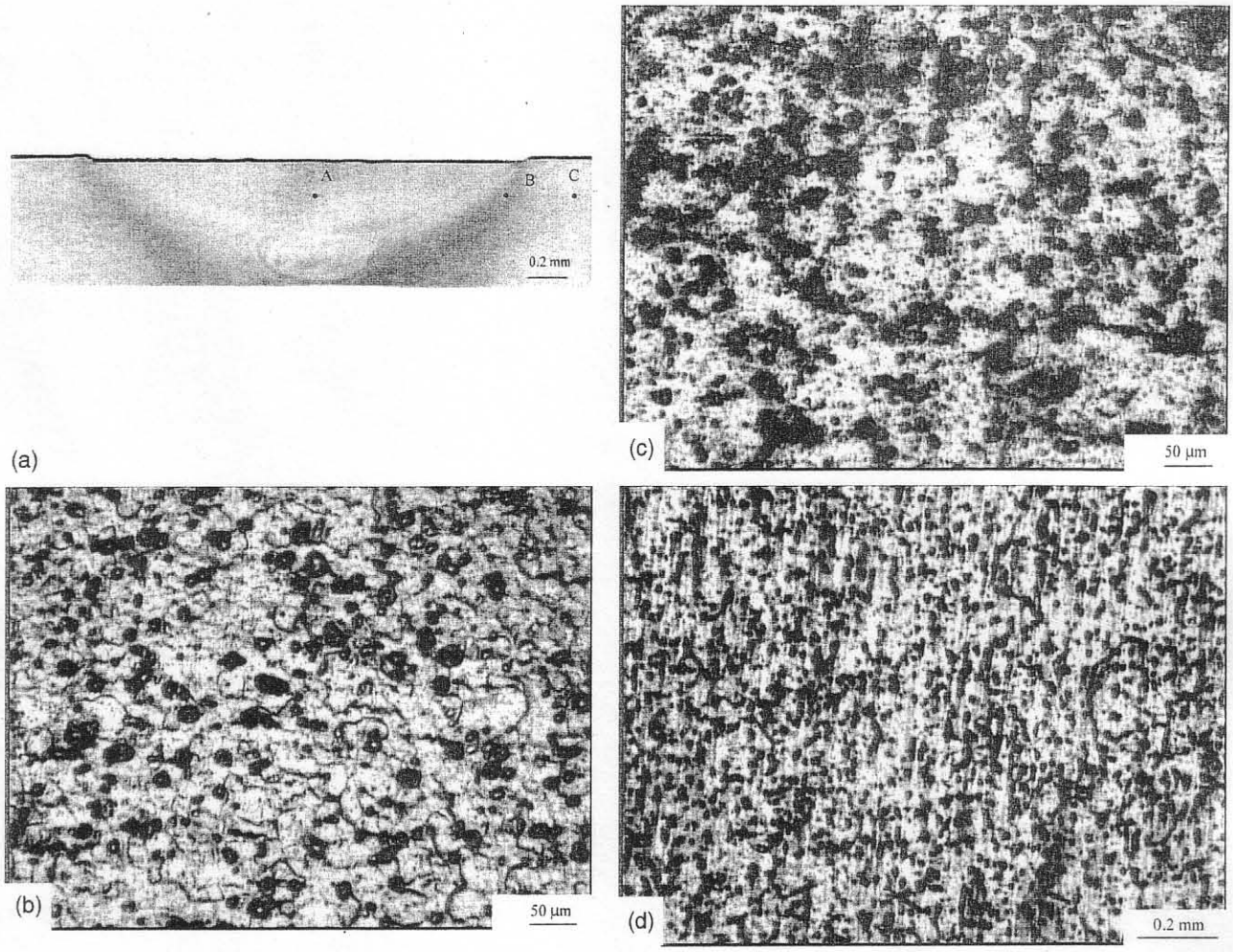

Fig. 4. Typical features of friction stir welded 6061-Al alloy; (a) weld cross section perpendicular to the welding direction; (b) equiaxed grains in the nugget zone around the position A; (c) heat-affected zone (HAZ) around the position B; (d) unaffected 6061-Al alloy in the position C.

6(a) shows the wavelet decomposition of the AE signals for the weld in a normal welding condition. Fig. 6(b) shows the WT decomposition of the AE signal acquired at the time the probe travels to the front edge of the first gap. The result of the wavelet transformation is a series of decomposed signals belonging to different frequency bands. The plots in Fig. 6(a,b) shows that A6 can be regarded as the result of passing signals $x(t)$ through a low-pass filter, with a resulting frequency bandwidth [0, 15.625 kHz]. D1–D6 correspond to the frequency bandwidths [15.625, 31.25 kHz], [31.25, 62.5 kHz], [62.5, 125 kHz], [125, 250 kHz], [250, 500 kHz], and [500, 1000 kHz], respectively. Comparing the plots in Fig. 6(a,b), it is seen that the intensity of D3 for welds with a gap defect increases around 60% of that for normal welds. The similar phenomena happened to A6, D1, D2, D4, D5 and D6; although; the degree of variation is different at different scales. The band energy computed by Eq. (1) shows in Figs. 3 and 5 that the energy is concentrated at scale 3 (with a bandwidth [62.5, 125 kHz]).

Both the three-dimensional representation and contour map of the wavelet transform for a weld with the gap defects are shown in Fig. 7. It is obvious that the general trend of the band energy peaks reflects the location and the size of the gap. The three relatively higher peaks located at 12, 27 and 42 s, respectively, match the moments when the probe traverses to the front-edge positions of the three gaps, correspondingly. The end edges of the three gaps correspond to relatively lower energy levels compared to the corresponding front edges. The plots in Fig. 7 also reveal an increase trend in energy with the increase of the gap size.

More detailed information is revealed in Fig. 8 which depicts the relation of band energy vs time at different scales. In-depth examination of the plots shows that the positions (a) and (e) shown in the Fig. 8 correspond to the moments when the front edge and the end edge of the shoulder pass over the front edge of the first gap, respectively. Peak (c) corresponds to the probe movement to the front edge of the first gap. The shoulders shown beside the main peak (c) are thought to be caused by the interaction between the edges of the probe and the first gap.

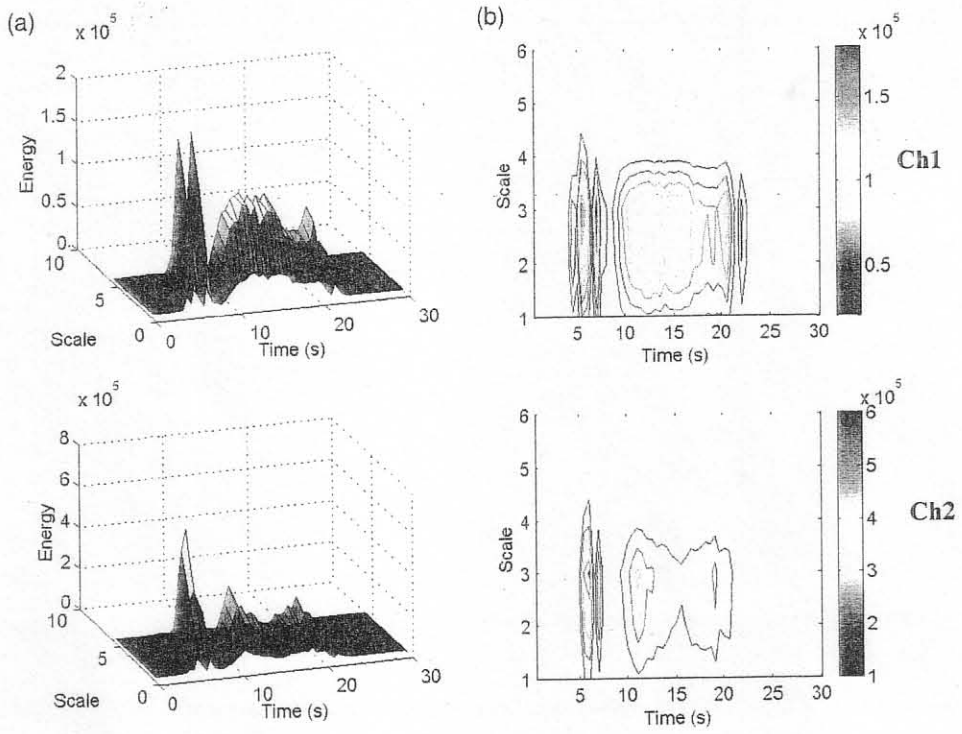

Fig. 5. The three-dimensional profile (a) and contour map of band energy vs time and scale (b) through WT of AE waveforms (for the entire FSW static process).

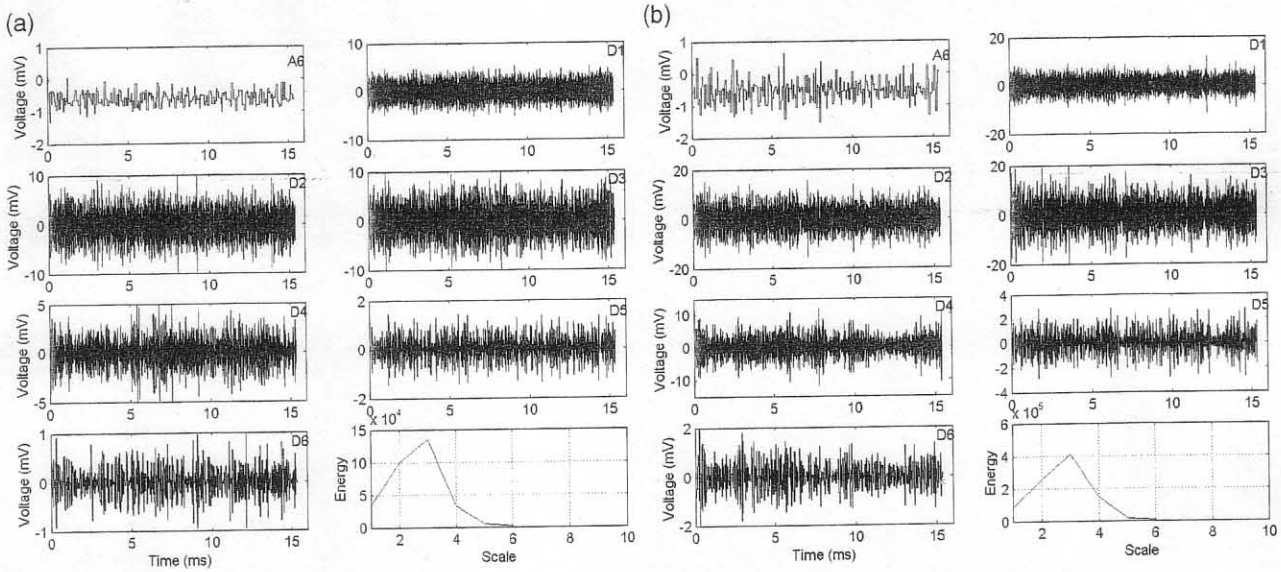

Fig. 6. WT decomposition of AE signals (channel 2) acquired at the time (a) the shoulder begins to pass the front edge of the first gap (t = 8 s) and (b) the probe traverses to the front edge of the first gap (t = 12 s).

The variation of the AE intensity in Fig. 8 can be explained as follows. As it is well known, the main heat source of FSW is the friction between the shoulder and top surface of the workpiece, and between the probe and materials around it. The AE signals are derived mainly from the friction between the tool and material, and thermoactivated deformation in the materials. At the beginning stage of welding after a full penetration of the probe into the material is completed, high friction between the cold material and the shoulder yields a large amount of heat to activate high energy defects and migrate grain boundaries, which consequently causes a large increase in AE intensity indicated by the first peak in Fig. 8. Afterwards, the degradation in the AE signal reflects cer-

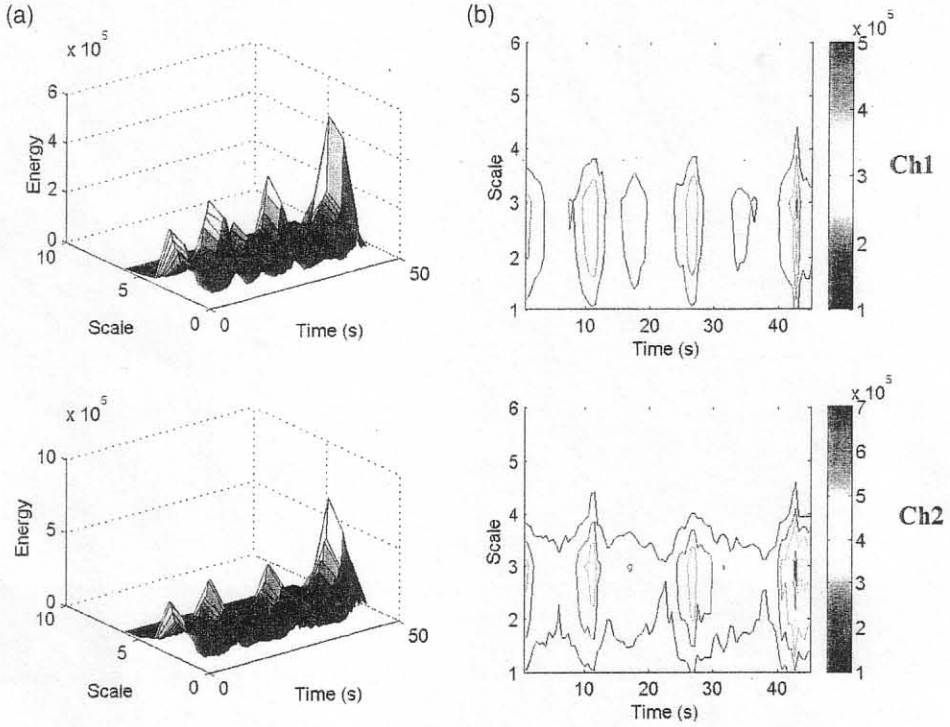

Fig. 7. Three-dimensional profile (a) and contour map of wavelet transform (b) for the weld with gap defects.

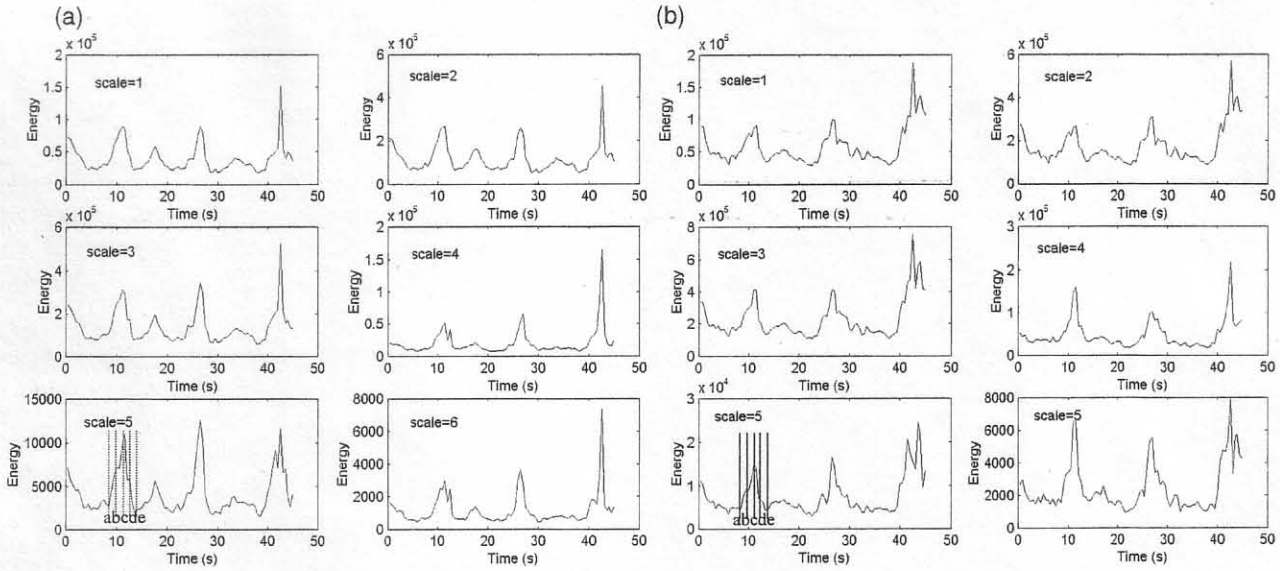

Fig. 8. Plots of band energy vs time at different scales for weld with gap defects. (a) channel 1, (b) channel 2.

tain features of the recrystallization in the expanding heat-affected zone. The AE intensity begins to increase while the periphery of the shoulder travels to the front edge of the first gap (indicated in Fig. 8a); at which point, the deformation and stress relief are believed to increase until the probe traverses to the front edge of the first gap. The AE intensity reaches the maximum value at (c) indicated in Fig. 8, then decreases due to the smaller friction zone between the tool and the gap-defected material until the front edge of the shoulder traverses to the end edge of the first gap. A similar phenomenon also happens to other main peaks at each scale; although little differences are present, and the above explanations also apply.

To provide for a comparison with AE features for the gap-defected weld, WT transforms of the AE for the welding of the butted plates without gaps are presented in Fig. 9. It is seen from Fig. 9 that the absolute values

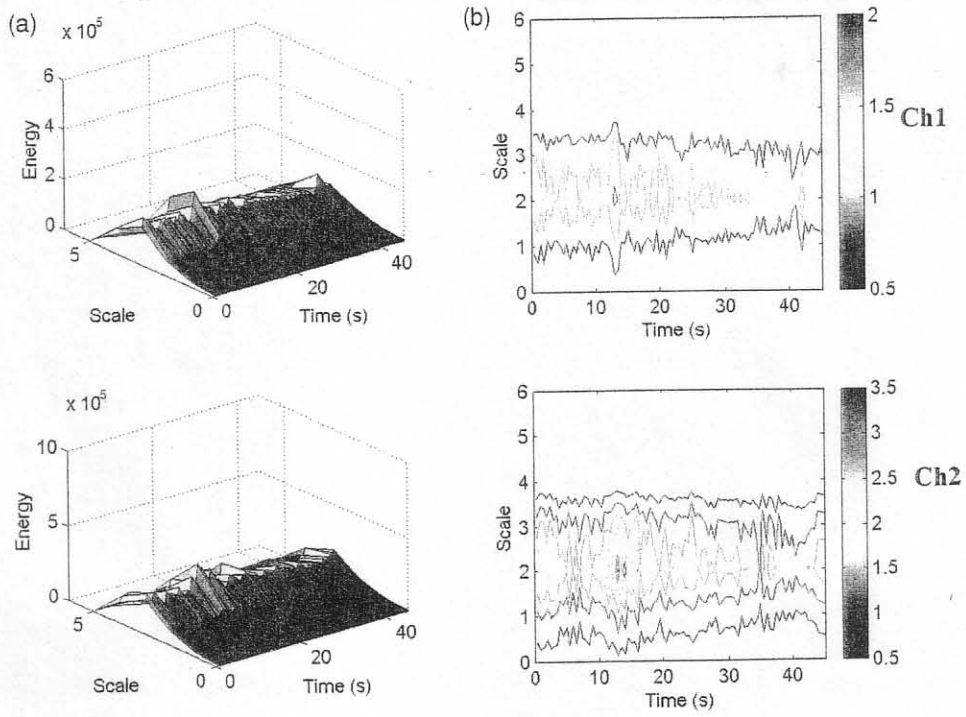

Fig. 9. Three-dimensional profile (a) and contour map of wavelet transform (b) for the weld with normal plate condition.

and the variations of the band energy for the plates without gaps are smaller compared with those for the welding of the gap-defected plates. From the discussion above, it is concluded that the existence of a fairly consistent AE band energy variation at every scale suggests that it is possible to predict the welding state and gap defect formation in FSW by monitoring the AE signal.

5. Conclusions

The fast response and high signal-noise-ratio of the AE signals can play an important role in the on-line monitoring of the FSW process. A wavelet transform of AE signals provides plots of frequency spectra vs time. The plots are very useful in the recognition of the AE features through a two-dimensional contour map and a three-directional profile of band energy. As different types of defects may yield different AE features in a specific range of frequencies, band energy variation during welding would provide a more detailed indication of the gap-induced defects compared to the total energy variation, and can also be useful in detecting the welding state transition during friction stir welding.

Acknowledgements

The authors are grateful for the financial support of the U. S. Department of Education, Grant No. P200A80806-98, and the American Welding Society, and also thankful to Mr Michael Valant for the technical assistance in preparing the experiments.

References

[1] C.J. Dawes, W.M. Thomas, Friction stir process for aluminum alloys, Welding Journal 75 (1996) 41–45.
[2] A.P. Reynolds, W.D. Lockwood, T.U. Seidel, Processing-property correlation in friction stir welds, Materials Science Forum 331-337 (2000) 1719–1724.
[3] D.A. Dornfeld, Design and Implementation of in-process sensors for the control of precision manufacturing processes, in: Advanced NDE Techniques for Process Sensing and Control, The American Society for Nondestructive Testing Inc., 1998, pp. 125–150.
[4] D. Dornfeld, Application of acoustic emission techniques in manufacturing, NDT & E International 25 (1999) 259–269.
[5] T. Tanaka, A. Okitsu, Diagnostic sensing of tool wear by spectrum analysis of interrupted cutting forces, Bulletin of the Japan Sociecty of Precision Engineering 13 (1979) 45–46.
[6] K. Matsuoka, D. Forrest, M.K. Tse, On-line wear monitoring using acoustic emission, Wear 162-164 (1993) 605–610.
[7] H.K. Tönshoff, M. Jung, S. Männel, W. Rietz, Using acoustic emission signals for monitoring of production processes, Ultrasonics 37 (2000) 681–686.
[8] C.K. Chui, An Introduction to Wavelets, Academic Press, New York, 1992.
[9] M. Song, R. Kovacevic, Numerical and experimental study of the heat transfer process in friction stir welding, Proceedings of the Institution of Mechanical Engineers B: Journal of Engineering Manufacture 217 (2003) 73–85.
[10] V.A. Plotnikov, Acoustic emission during heating of strained aluminum, Technical Physics Letters 27 (2001) 27–32.
[11] L.E. Murr, G. Liu, J.C. McClure, A TEM study of precipitation and related microstructures in friction-stir-welded aluminum, Journal of Materials Science 33 (6061) (1998) 1243–1251.